Solar Energy Materials & Solar Cells 113 (2013) 160–164

Contents lists available at SciVerse ScienceDirect

Solar Energy Materials & Solar Cells

journal homepage: www.elsevier.com/locate/solmat

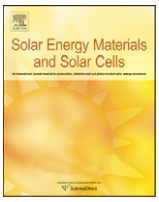

The effect of Zn excess on kesterite solar cells

Wan-Ching Hsu [a], Ingrid Repins [b,*], Carolyn Beall [b], Clay DeHart [b], Glenn Teeter [b], Bobby To [b], Yang Yang [a,**], Rommel Noufi [b]

[a] Department of Materials Science and Engineering, University of California, Los Angeles, CA 90095, USA
[b] National Renewable Energy Laboratory, Golden, CO 80401, USA

ARTICLE INFO

Article history:
Received 22 August 2012
Received in revised form
21 January 2013
Accepted 16 February 2013
Available online 15 March 2013

Keywords:
CZTS
Kesterite
Thin film
Solar cell
Co-evaporation
Earth-abundant

ABSTRACT

Accuracy in composition control has been one of the top issues for fabricating high-performance kesterite ($Cu_2ZnSn(Se,S)_4$) solar cells. A detailed understanding of the effect of Zn excess on device performance has not yet been demonstrated. Thus, specific criteria for high-performance devices, in particular discriminating between the effects of Zn-rich features at the front versus the back of the absorber, are desired. In this study, we report that co-evaporated kesterite absorbers can demonstrate high device efficiency despite the presence of large quantities of ZnSe. However, the benign presence of ZnSe is found to be conditional. While large ZnSe grains on the back of the absorbers are not harmful to device performance, the ZnSe grains produced by excess Zn near the end of the deposition degrade the cell efficiency from 8% level to 6% level (without anti-reflection coatings). The other effect related to excess Zn on the front of absorber is the facilitation of breakdown in lower reverse bias. The breakdown indicated here occurs only under the illumination of blue photons, and to our best knowledge has not been reported before. The exact mechanism of the breakdown remains open, but it is demonstrated to be related to the photoconductivity of CdS, and is thus possibly a symptom of lateral defect issues in the absorber, caused by the overdose of Zn. The same type of issue contributing to the breakdown may also be responsible for part of the parasitic loses at the working voltage, and therefore warrants further research.

1. Introduction

Earth-abundant kesterite ($Cu_2ZnSn(Se,S)_4$) solar cells, which have great structural similarities to chalcopyrite ($Cu(In,Ga)Se_2$), have achieved successful cell efficiency around 10%. A recent summary of the deposition techniques and results can be found elsewhere [1]. Even though the kesterite and chalcopyrite structures are both based on zincblende, the kesterite is known to be less tolerable in composition: it exhibits only a small single-phase region in the equilibrium phase diagram, according to experimental [2] and computational [3] results. Venturing out of this region leads to the formation of numerous binary and ternary phases such as $Cu_{2-x}S$, ZnS, SnS_x, and Cu_2SnS_3, or their selenide counterparts. Extremely precise composition control is not straight-forward for most of the existing processing today, including evaporation, sputtering, and ink-based approaches, due to limited accuracy of deposition rate control and/or the volatile nature of the numbers of elements and precursor phases. Therefore, it is valuable to quantitatively assess the impact of off-stoichiometry and common secondary phases.

Most studies to date have found their most efficient cells at compositions around $Cu/(Zn+Sn)=0.9$ $Zn/Sn=1.25$ and along the line between kesterite phase and ZnX phase in the CuX–ZnX–SnX_2 (X=S or Se) ternary phase diagram [4]. It is detrimental to go away from this line toward the Cu-rich regime, since Cu_xSe_y is notorious as semi-metallic phases that short the device. It is slightly tolerable to go below the line, gaining more Sn in composition, but the limit is still strict, possibly because of the various Sn-related deep traps predicted by first principle calculations [5]. The Zn-rich direction along the line is the only direction that has not been found to be disastrous for device performance. A very Zn-rich composition results in the segregation of ZnS/ZnSe, which has a large negative formation energy [6]. A large amount of ZnS has been observed on the back of an 8.4% Cu_2ZnSnS_4 solar cell [7] and was thus deemed electrically unimportant. However, in another study [8], a reduction of cell efficiency by half has been ascribed to 24 volume % of ZnS in the Cu_2ZnSnS_4 absorber. On the other hand, localized Zn-rich composition could be beneficial to devices. In the studies of coevaporated $Cu_2ZnSnSe_4$ by NREL, it is found that a thin Zn-rich cap on the surface of the absorber enhances the open-circuit voltage (Voc), short-circuit current

* Corresponding author. Tel.: +1 303 384 7678; fax: +1 303 384 7600.
** Corresponding author. Tel.: +1 310 825 4052; fax: +1 310 206 7353.
E-mail addresses: ingrid.repins@nrel.gov (I. Repins), yangy@ucla.edu (Y. Yang).

0927-0248/$ - see front matter © 2013 Elsevier B.V. All rights reserved.
http://dx.doi.org/10.1016/j.solmat.2013.02.015

density (Jsc), and fill factor (F.F.) [9]. Considering the discrepancy within the literature, more specific criteria for the presence or lack of ZnSe/ZnS in efficient kesterite devices are desired.

2. Absorber co-evaporation and device fabrication

$Cu_2ZnSnSe_4$ thin films were deposited by co-evaporation of elemental Cu, Zn, Sn, and Se on Mo-coated sodalime glass with a 150 Å layer of e-beam evaporated NaF precursor. The substrate temperature was set to 495–505 °C to allow immediate reaction between precursors. The deposition recipes are modified from previous published recipes. Details of a sample deposition on elemental deposition rates, temperature profiles, working pressure, and cooling down conditions can be found in Ref. [9]. In this study, in order to intentionally create Zn excess at the front of absorber films, additional Zn evaporation flux was applied at the end of depositions, specifically 5 min longer than the usual termination time. To create Zn excess on the back of absorber films, instead, a relative high Zn flux was applied from the beginning of depositions. Also we made sure the Cu and Sn supplied later in the deposition were not sufficient to transform the as-formed Zn excess phase on the bottom into kesterite. (The SEM images published in Ref. [10] shows the formation of ZnSe grains in the earlier stage of deposition and the consumption of them in the later stage when enough Cu and Sn were deposited.) For all the depositions, a small amount of Zn (about 250 Å) was applied as the substrate was cooled to 430 °C to create the performance-enhancing "Zn cap" mentioned in [9].

Absorbers were also subjected to a 175 °C in air-anneal, described in previous work [9]. For a study of the possible relationship between the air anneal and Zn at the front of the device, neighboring pieces of the same absorber were finished into devices with and without the air anneal.

The device structure is identical to the commonly-used structure of CIGS solar cells: a chemical-bath-deposited CdS, a sputtered resistive/conductive ZnO bi-layer, e-beam-evaporated Ni/Al grids, and photolithographic device isolation. MgF_2 AR coatings were not applied unless mentioned specifically.

3. Film and device characterization

The bulk compositions of films were obtained by X-ray fluorescence spectroscopy (XRF). Auger emission spectroscopy (AES) was used for composition depth profiles, with the sensitivity factors calibrated by XRF. Locations of ZnSe grains were identified from cross-sectional SEM images [11] and AES depth profile.

Internal quantum efficiencies (QE_{INT}) were calculated from measuring external quantum efficiency (EQE) and reflectance (R) as $EQE/(1-R)$. The reflectance was obtained from the non-gridded area on samples.

4. The effect of ZnSe position on device performance

It has been demonstrated both by the authors and in the literature that high efficiency devices may be produced with a wide range of Zn contents. Table 1 is a list of the best $Cu_2ZnSnSe_4$ devices fabricated by the same evaporator at NREL within each specified range of composition. Their actual compositions and deposition run numbers are also provided. Compositions ranging from 26.9% to 37.1% in Zn/(Cu+Zn+Sn) ratio are mostly capable of producing effective devices in 8% level before AR coating. AR coating reproducibly increases the PCE by 5–10% relative. Since some of the films are extremely rich in Zn, there is no doubt that a large quantity of ZnSe coexists with kesterite in these efficient devices. Formation of metallic Zn is not possible because it is volatile in vacuum at the deposition temperature (around 500 °C).

Table 1
Best NREL co-evaporated $Cu_2ZnSnSe_4$ devices within the specified range of composition before AR coating. The Zn/(Cu+Zn+Sn) of stoichiometric $Cu_2ZnSnSe_4$ is 25%. 8.45% device can be made even the film contains Zn/(Cu+Zn+Sn) as high as 37.0%. The PCEs of M3512 and M3464 after AR coating are shown in brackets.

Zn/(Cu+Zn+Sn) (%)	Best PCE in the ranges (%)	Actual Cu, Zn, Sn/(Cu+Zn+Sn) (%)	Run numbers
35	8.45	42.5, 37.0, 20.5	M3490
33–35	7.34	43.7, 33.8, 22.5	M3433
31–33	8.21	44.2, 32.6, 23.2	M3480
29–31	8.55 (w/AR 9.26%)	46.0, 30.0, 24.0	M3512
27–29	8.75 (w/AR 9.15%)	45.9, 28.6, 25.5	M3464
25–27	8.22	46.5, 26.9, 26.6	M3503

A more specific description on the status of ZnSe grains is desired. Cross-sectional SEM images and AES depth profiles provide the positions of ZnSe in the film. Six films were studied in details. In the SEM images shown in Fig. 1(a), bright features are observed either on the top or the bottom of the film. With multiple confirmations by EDS, we are convinced that these features are grains of ZnSe which appears bright because of charging effect of a less conductive phase [11]. The films in category (I) (M3530, M3503) have a small but observable amount of bright spots on the top of the film as a result of the Zn cap mentioned earlier. Besides this Zn-rich layer on the top surface, no larger grains of ZnSe can be observed across the two films. For category (II) (M3480, M3490), in addition to the Zn cap, submicron to micron sized ZnSe grains are observed on the back of the films. All the other devices listed in Table 1 have cross-sectional images belong to either this category if it is rich enough in Zn, or category (I) if not rich enough. For category (III) (M3531, M3463), ZnSe grains up to 300 nm in diameter are observed on the front of the films and protrude somewhat into the film along grain boundaries.

The distribution of Zn in the AES depth profiles further confirms the ZnSe positions observed by SEM images. One depth profile of Zn/(Cu+Zn+Sn) and Se/(Cu+Zn+Sn) out of each category is shown in Fig. 1(b). Compared to the stoichiometric ratio of $Cu_2ZnSnSe_4$, the profiles are all Zn-rich throughout the films and even richer on the very surface of the films. The film shown representative of category (II) has an additional Zn-rich section near the Mo back contact, while the Zn-rich region for the category (III) film is on the front and penetrates more deeply into than that of the other two. The above description matches the observation of ZnSe locations from SEM images. In addition, the composition of Cu, Zn, and Sn (Cu and Sn are not shown in the paper) in the middle section of the profiles is relatively flat and exhibits little difference between three films. Since ZnSe grains are not located in the bulk of the film and SnSe, $SnSe_2$, Cu_2SnSe_3, and Cu_2SnSe_4 either evaporates or decomposes on high-temperature substrates (around 500 °C) [9,10], the average AES composition derived from the middle section of the film can be attributed to the phase composition of $Cu_2ZnSnSe_4$, namely Zn/(Cu+Zn+Sn)=0.265, Cu/(Cu+Zn+Sn)=0.475 (identical to Cu/(Zn+Sn)=0.94, Zn/Sn=1.03). This composition is marked in the ternary phase diagram shown in Fig. 2 together with the composition of the six films. Until now, we have not found efficient devices with bulk composition poorer in Zn than this phase composition.

With better understanding on the position of ZnSe for these specific films, the effect of ZnSe position on their device performance now may be discussed. By comparing the J–V parameters

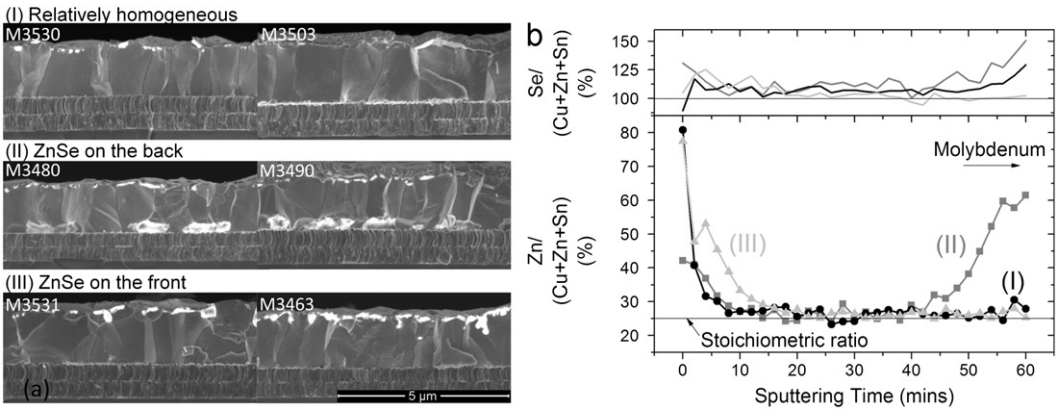

Fig. 1. (a) Cross-sectional SEM images of films with: (I) relatively homogeneous composition (M3530, M3503); (II) ZnSe grains on the back (M3480, M3490); (III) ZnSe grains on the front (M3531, M3463). (b) Depth profiles of Zn/(Cu+Zn+Sn) ratio derived from AES depth profile of: (I)M3530; (II)M3490; and (III)M3531.

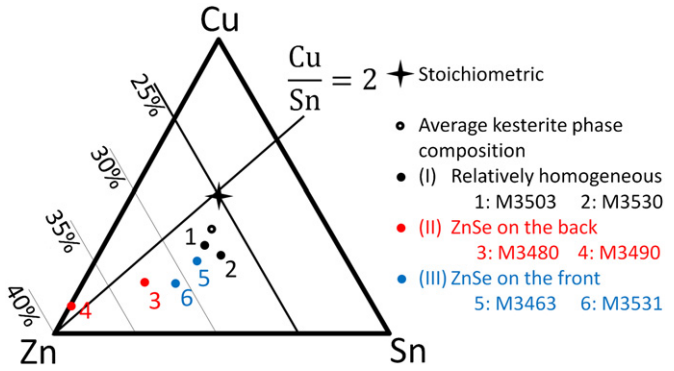

Fig. 2. Compositons of the mentioned films obtained from XRF. Until now, we have not found efficient devices with bulk composition poorer in Zn than this phase composition.

of devices listed in Table 2, it is found that when the amount of Zn is controlled well to that corresponding to single-phase kesterite (such as for samples M3530 and M3503), the cell efficiency attains ~8% without antireflection coating. If the film is much richer in Zn, and the ZnSe particles precipitate on the back of the absorber layer (such as for samples M3480 and M3490), the device performance is not affected. However, devices with large ZnSe grains on the front of the absorber layer have a much lower performance. Category III sample M3531, with a 6.51% efficiency, was deposited with deposition conditions identical to that of 8.28%-efficient category I sample M3530, except for the additional amount of Zn was added at the end of deposition. The reduced J_{sc} shown in Table 2 is responsible for half of the cell efficiency loss between these two samples, and the other half is due to the deficiency in V_{oc} and F.F. The internal quantum efficiency (QE_{INT}) shown in Fig. 3(a) is defined as $EQE/(1-R)$, where R=reflectance of devices. From M3530 to M3531, the loss in current is relatively independent of wavelength according to the QE_{INT} ratio shown in the same figure. The fact that the ratio between QE_{INT} of M3531 and QE_{INT} of M3530 does not decrease with longer wavelength suggests an issue locating on the front of the absorber instead of the bulk: bulk issues typically introduce difficulty in carrier collection from the back of the absorber, thus producing a stronger red than blue loss. The loss mechanism is therefore consistent with the observation of large ZnSe grains on the *front* of M3531. One possible reason behind the ZnSe position-sensitive current is a differential carrier blocking ability to electrons versus holes. ZnSe on the front of the absorber blocks electron and as a result reduces the photocurrent, while hole blocking by ZnSe on the back is negligible.

5. Blue-light induced breakdown

Reverse voltage diode breakdown is apparent in all the light *JV* data of Fig. 3(b), and is particularly severe in the category III (excess Zn at front) air-annealed devices. For the air-annealed category III devices, the breakdown occurs even in the dark *JV* data, and in the light JV data occurs at a smaller reverse voltage than for the other types of devices. In contrast, air-annealing a relatively homogeneous film did not make considerable change to *JV* (M3530-a). Therefore, we conclude that the severity of the breakdown behavior is related to the excess of Zn on the front of the absorbers and appears obvious when the extra Zn layer is oxidized.

Air-annealed category III devices not only show increased reverse bias breakdown, but also severely decreased performance. The *J–V* parameters of M3530, M3530-a, M3531, and M3531-a are given in Table 2. The parameters of M3530-a and M3531-a are presented in parentheses after those of M3530 and M3531, respectively. The absorbers of M3530-a and M3531-a were cut from the same piece of M3530 and M3531, respectively, but were annealed at 175 °C for 5 min in air. While the device with relatively homogeneous composition (M3530) has only a slight reduction in cell efficiency, the one with excess Zn on the front of absorber (M3531) suffers from large degradation to Voc, Jsc, and F.F., resulting in a great reduction of device efficiency (to 4.68%). Thus, we are motivated to further study the reverse voltage breakdown, not only to understand the role of Zn at the front of the device, but also because the most severe breakdown occurs in the devices with the poorest performance. Understanding and eliminating the effect may therefore help improve performance.

J–V measurements under the illumination of different wavelength ranges were conducted to study the mechanism of breakdown behavior. Fig. 4(a) shows the results of simulated AM1.5 filtered by 570 nm, 530 nm and 495 nm long-pass filters, along with unfiltered white light. It appears that the breakdown is blue light-sensitive as the breakdown does not appear when the light is filtered by 570 long-pass filter. To understand the response of breakdown with better resolution in photon energy, reverse bias QE was measured. Data are shown in Fig. 4(b). At reverse biases below 1.0 V, the QE basically retraces the unbiased QE with slight enhancement at long wavelengths. Beyond 1.0 V, a peak appears between 360 nm and 530 nm. The magnitude of the peak rises abruptly with slight increase in the reverse voltage. It is important to realize that an apparent quantum efficiency exceeding 100% does not indicate actual generation of more carriers than photons incident. Rather, the reverse-biased QE measures the vertical distance (current) between light and dark *JV* curves at a

Table 2
J–V parameters of devices, PCE, Voc, Jsc, and F.F. Numbers in parentheses are results obtained after annealing bare absorber.

Zn contents	Run numbers	PCE (%)	*Voc* (mV)	J_{sc} (mA/cm$^{2)}$	F.F. (%)
~Phase composition	M3503	8.22	351	35.9	65.3
	M3530(-a)	**8.02(7.77)**	**359(357)**	**34.4(34.0)**	**64.9(64.0)**
> Phase composition ZnSe on the back	M3480	8.21	360	36.1	63.1
	M3490	8.45	376	34.0	66.1
> Phase composition ZnSe on the front	M3463	6.60	338	31.7	61.7
	M3531(-a)	**6.51(4.68)**	**337(321)**	**31.5(28.6)**	**61.3(51.0)**

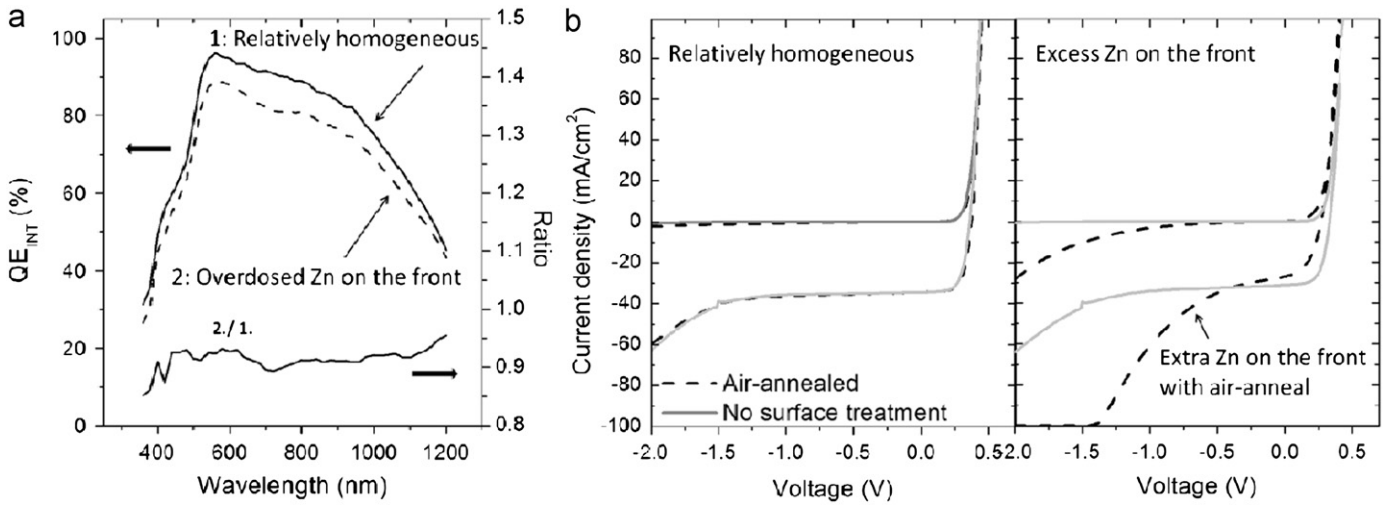

Fig. 3. (a) QE_{INT} of cells without large ZnSe grains (category I, M3530), with ZnSe grains on the front of absorber (category III, M3531) and the ratio between the two. (b) *JV* curves of the same two devices (M3530, and M3531) and their air-annealed counterparts (M3530-a, M3531-a).

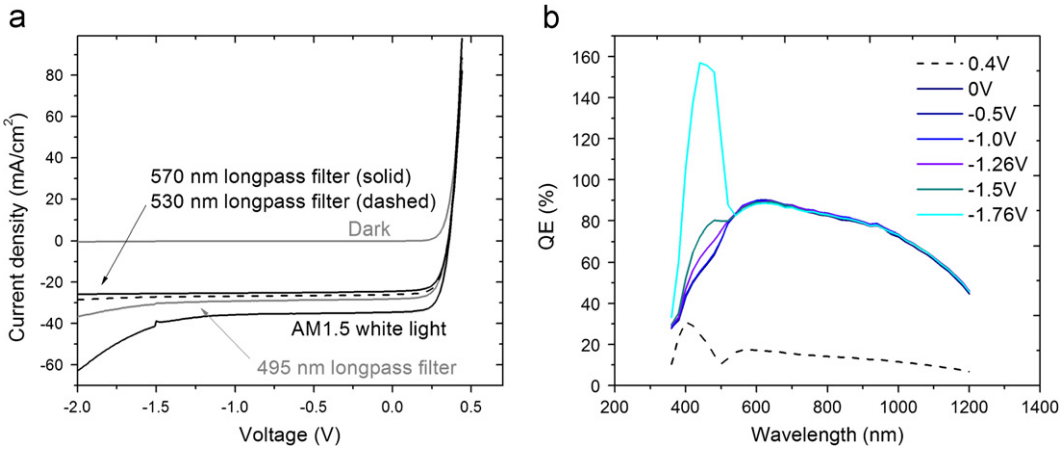

Fig. 4. (a) *JV* curves measured under the illumination of simulated AM1.5 with different optical filters, and (b) non-equilibrium QE of M3530.

given bias. Thus, the large apparent QE is an indicator of the light-activated breakdown or shunting.

The absorption edge to turn on the breakdown is identified as 530 nm by the leading edge of the peak in the QE. This analysis agrees with the findings from JV curves that a 495 nm long-pass filter does not turn off the breakdown, and a 530 nm filter nearly does. 530 nm matches accurately with the absorption edge of CdS [12]. Accordingly, the blue-photon induced breakdown is likely to be associated with the absorption of CdS. The 530 nm onset of the breakdown does *not* match with the absorption of ZnSe, even though it exists in large quantities for devices where the breakdown effect is most severe. Optical effects in ZnSe are expected to appear around 460 nm, based on the larger band gap of ZnSe. In addition, in the forward-biased QE, the wavelength onset of the peak (shown in Fig. 4(b), 0.4 V) matches well with that of a CIGS device with CdS as buffer layer [14] and fails to match with the one with ZnSe as buffer layer [15]. The photoconductivity of CdS has been previously reported in CIGS solar cells to result in the distortion of light *JV* curves in the fourth (power) quadrant under certain conditions [13]. This work is the first report of a blue-photon sensitive non-linear effect in the third quadrant.

One simple model that could possibly help us to understand how the behavior is related to CdS photo-conductance is the lateral distribution of shunting channels. When shunting channels

are laterally distributed on absorber, the current will be switched on when CdS is illuminated, turns conductive, and provides little spreading resistance for the current exiting the shunt paths. In this case, even though a simple metallic shunting behavior is sufficient to explain the on and off characteristics of the reverse current, it is still not enough to explain the magnitude of the reverse current being non-linear with voltage. In essence, the breakdown behavior is a result of problematic absorber which has lateral distributed defects and those defects must have non-Ohmic contacts with photoconductive CdS.

The actual chemistry of these defects remains unclear to us. As described, the severity of blue-photon induced breakdown is related to the excess of Zn at the front of absorber. Therefore, even though ZnSe's absorption does not directly result in the behavior (instead, the absorption of CdS does), an effect involving both the absorption of CdS and the excess of Zn must be responsible. It has been demonstrated in the SEM images that, for category III films, the Zn excess produces grains of ZnSe that protrude into kesterite films along the grain boundaries. The penetration of excess Zn may at the same time produces other types of Zn-rich features along the grain boundaries. Alteration of the localized electrical property is possible. Air-anneal converts ZnSe on the surface into ZnO, which has much lower conduction band edge[16], and thus may facilitate current flow. The hidden electrical defects are accordingly exposed, exhibiting as severe breakdown and reduced F.F.

In brief, we think the blue-light induced breakdown is a symptom of problematic absorbers. The generation of Zn-rich localized features followed by air-annealing is one of the ways to create or activate these defects. The same type of defect contributing to the breakdown may be responsible for part of the parasitic loses at the PV working voltage as well and therefore deserves certain degree of attention.

6. Conclusion

We report co-evaporated $Cu_2ZnSnSe_4$ devices in the 8% to 9% efficiency range made from absorbers with a wide range of Zn/(Cu+Zn+Sn) ratio. This Zn/(Cu+Zn+Sn) ratio extends up to 37.1%, which is almost 1.5 times of the stoichiometric Zn content, and far beyond the commonly-stated composition standard, Cu/(Zn+Sn)=0.9 Zn/Sn=1.25. We further found that not every absorber that is very rich in ZnSe is able to yield good cell efficiency. It is required that the ZnSe grains are at the back of the device. Large ZnSe grains on the front of the absorber, created by overdosing Zn at the end of deposition, are detrimental for device performance.

We also observe a blue-light induced reverse-bias breakdown. The breakdown is more severe with a large excess of Zn in the end of deposition, yet the wavelength onset of the breakdown matches with the CdS bandgap. Qualitatively, the effect is considered as a symptom of lateral distributed defect in the absorber (in this case ZnSe grains protruding into the absorber) through which current is regulated by the spreading resistance of the CdS.

Acknowledgment

The Authors thank Kitty Cha for proof-reading the manuscript.

References

[1] C.M. Fella, A.R. Uhl, Y.E. Romanyuk, A.N. Tiwari, $Cu_2ZnSnSe_4$ absorbers processed from solution deposited metal salt precursors under different selenization conditions, Physica Status Solidi A 6 (2012) 1043–1048.
[2] I.D. Olekseyuk, I.V. Dudchak, L.V. Piskach, Phase equilibria in the Cu_2S–ZnS–SnS_2 system, Journal of Alloys and Compounds. 368 (2004) 135–143.
[3] S. Chen, X.G. Gong, A. Walsh, S.-H. Wei, Defect physics of the kesterite thin-film solar cell absorber Cu_2ZnSnS_4, Applied Physics Letters 96 (2010) 021902.
[4] H. Katagiri, K. Jimbo, M. Tahara, H. Araki, The influence of the composition ratio on CZTS-based thin film solar cells, Materials Research Society Symposium Proceedings 1165 (2009) M04–01.
[5] S. Chen, J.-H. Yang, X.G. Gong, A. Walsh, S.-H. Wei, Intrinsic point defects and complexes in the quaternary kesterite semiconductor Cu_2ZnSnS_4, Physical Review B 81 (2010) 35–37.
[6] J.J. Scragg, P.J. Dale, D. Colombara, L.M. Peter, Thermodynamic Aspects of the synthesis of thin-film materials for solar cells, Chemphyschem: A European Journal of Chemical Physics and Physical Chemistry 13 (2012) 3035–3046.
[7] B. Shin, O. Gunawan, Y. Zhu, Thin film solar cell with 8.4% power conversion efficiency using an earth-abundant Cu_2ZnSnS_4 absorber, Progress in Photovoltaics: Research and Applications 21 (2013) 72–76.
[8] J. Just, D. Lutzenkirchen-Hecht, R. Frahm, S. Schorr, T. Unold, Determination of secondary phases in kesterite Cu_2ZnSnS_4 thin films by X-ray absorption near edge structure analysis, Applied Physics Letters 99 (2011) 262105.
[9] I. Repins, C. Beall, N. Vora, C. DeHart, D. Kuciauskas, P. Dippo, B. To, J. Mann, W.-C. Hsu, A. Goodrich, R. Noufi, Co-evaporated $Cu_2ZnSnSe_4$ films and devices, Solar Energy Materials and Solar Cells. 101 (2012) 154–159.
[10] W.-C. Hsu, I. Repins, C. Beall, C. DeHart, B. To, W. Yang, Y. Yang, R. Noufi, Growth mechanisms of co-evaporated kesterite: a comparison of Cu-rich and Zn-rich composition paths, Progress in Photovoltaic: Research and Applications, http://dx.doi.org/10.1002/pip.2296, in press.
[11] N. Vora, J. Blackburn, I. Repins, C. Beall, B. To, J. Pankow, G. Teeter, M. Young, R. Noufi, Phase identification and control of thin films deposited by co-evaporation of elemental Cu, Zn, Sn, and Se, Journal of Vacuum Science & Technology A: Vacuum Surfaces, and Films 30 (2012) 051201.
[12] S. Ninomiya, S. Adachi, Optical properties of wurtzite CdS, Journal of Applied Physics 78 (1995) 1183.
[13] A.O. Pudov, A. Kanevce, H.A. Al-Thani, J.R. Sites, F.S. Hasoon, Secondary barriers in CdS–$CuIn_{1-x}Ga_xSe_2$ solar cells, Journal of Applied Physics. 97 (2005) 064901.
[14] M. Köntges, R. Reineke-Koch, P. Nollet, Light induced changes in the electrical behavior of CdTe and Cu(In,Ga)Se_2 solar cells, Thin Solid Films 404 (2002) 280–286.
[15] B. Hahn, W. Gebhardt, W. Riedl, U. Rau, Cu(In,Ga)Se_2 solar cells with a ZnSe buffer layer: interface characterization by quantum efficiency measurements, Progress in Photovoltaics: Research and Applications 7 (1999) 423–436.
[16] S.B. Zhang, S.-H. Wei, A. Zunger, A phenomenological model for systematization and prediction of doping limits in II–VI and I–III–VI2 compounds, Journal of Applied Phyiscs 83 (1998) 3192–3196.